CARDIOVASCULAR DISEASE

Dynamic load modulation predicts right heart tolerance of left ventricular cardiovascular assist in a porcine model of cardiogenic shock

Kimberly K. Lamberti[1], Steven P. Keller[2], Elazer R. Edelman[1,3]*

Ventricular assist devices (VADs) offer mechanical support for patients with cardiogenic shock by unloading the impaired ventricle and increasing cardiac outflow and subsequent tissue perfusion. Their ability to adjust ventricular assistance allows for rapid and safe dynamic changes in cardiac load, which can be used with direct measures of chamber pressures to quantify cardiac pathophysiologic state, predict response to interventions, and unmask vulnerabilities such as limitations of left-sided support efficacy due to intolerance of the right heart. We defined hemodynamic metrics in five pigs with dynamic peripheral transvalvular VAD (pVAD) support to the left ventricle. Metrics were obtained across a spectrum of disease states, including left ventricular ischemia induced by titrated microembolization of a coronary artery and right ventricular strain induced by titrated microembolization of the pulmonary arteries. A sweep of different pVAD speeds confirmed mechanisms of right heart decompensation after left-sided support and revealed intolerance. In contrast to the systemic circulation, pulmonary vascular compliance dominated in the right heart and defined the ability of the right heart to adapt to left-sided pVAD unloading. We developed a clinically accessible metric to measure pulmonary vascular compliance at different pVAD speeds that could predict right heart efficiency and tolerance to left-sided pVAD support. Findings in swine were validated with retrospective hemodynamic data from eight patients on pVAD support. This methodology and metric could be used to track right heart tolerance, predict decompensation before right heart failure, and guide titration of device speed and the need for biventricular support.

INTRODUCTION

Mechanical circulatory support technologies have transformed critical care for patients with heart failure and acute cardiogenic shock, enabling native heart recovery by offering the potential to meet metabolic demands, maintain organ perfusion, and unload the failing left ventricle without markedly increasing oxygen consumption and demand on the native heart (1–4). As ventricular assist devices (VADs) are used more clinically, including surgically implanted durable VADs and percutaneous temporary VADs, unique challenges have arisen, particularly amplification of the limitations imposed by right ventricular tolerance to left-sided support. Traditionally, right-left ventricular coupling is a feature of intact cardiovascular homeostasis and enables the ventricles to support and counterbalance each other to maintain cardiac output (5–7). Successful left-sided VAD support requires that the right heart can match mechanically enhanced left-sided blood flow, despite the decoupling of native cardiovascular interactions, including right-left ventricular coupling, that is induced by VAD unloading. One of the critical challenges for VAD support of the left ventricle is the emergence of right ventricular dysfunction or failure in the acute period after initiation of left-sided support, which affects up to 43% of patients with left ventricular assist and is associated with higher in-hospital mortality (8–15).

The left and right ventricles are functionally coupled through intracardiac interactions and serial interactions across the closed-loop hemodynamic circuit (5). Intracardiac interactions consist of systolic

buttressing and diastolic interdependence through septal shift and compliance changes (5, 7, 16). Series interactions generate a link between right ventricular afterload and left ventricular preload through the pulmonary circulation. Emerging research emphasizes the influence of left ventricular loading state on right ventricular afterload and pulmonary vascular compliance and vice versa (17–19). Given that mechanical circulatory support disrupts native coupling across the cardiovascular system, VADs perturb not just the left ventricular but also the right ventricular loading state due to these right-left ventricular interactions. If the right heart is unable to compensate, then patients are at risk of right ventricular failure, diminished utility of mechanical circulatory support, and complete cardiovascular decompensation.

The role of the right ventricle as a limiting factor in left-sided mechanical support has been most appreciated in the context of durable VADs (12, 13, 15, 20–25). These devices are generally placed in patients with stable chronic heart failure, and right heart studies focus on the acute post-operative phase as patients recover from surgical device implantation (14, 26–36). However, percutaneous ventricular assist devices (pVADs) can be less invasively inserted and removed to provide temporary left ventricular support. Ease of insertion and extraction has reduced the threshold for use, and pVAD utilization has surpassed durable device use. There are 40,000 to 50,000 cases of cardiogenic shock annually in the United States alone, and use of temporary, short-term mechanical support to treat those patients is growing, with between 16 and 42.6% of cases supported in current analyses (3, 37–41). Emergence of right ventricular failure in the hours after initiation of left-sided pVAD support is caused by the right heart's inability to tolerate acute changes in loading state and to match mechanically enhanced left-sided output, not from long-term physiological adaptations. Right heart intolerance in general is further compounded by the wide variation and rapidly evolving acute cardiac dysfunction of patients in cardiogenic shock,

[1]Institute for Medical Engineering and Science, Massachusetts Institute of Technology, Cambridge, MA 02139, USA. [2]Pulmonary and Critical Care Medicine, Johns Hopkins University, Baltimore, MD 21205, USA. [3]Cardiovascular Medicine, Brigham and Women's Hospital, Harvard Medical School, Boston, MA 02115, USA.
*Corresponding author. Email: ere@mit.edu

such that the need to track and predict right heart state has become critical (*42–49*). Despite the clinical prevalence of right ventricular failure after acute left ventricular support, a critical hole remains—namely, that the physiologic basis of this occurrence in the acute setting is not fully understood and metrics to predict and track right ventricular decompensation are limited.

Here, we leverage the unique position of the indwelling, transvalvular pVAD to gain insight into the native cardiovascular response to left ventricular support. In a controlled porcine model of left ventricular ischemia and progressive right ventricular strain, we show that rapid pVAD speed sweeps generated a means of safely, dynamically stressing the heart—changing loads without loss of mechanical support. This assessment could not be achieved otherwise, as the indwelling pVAD simultaneously prevented systemic collapse and enabled accumulation of functional cardiac metrics. We report clinically accessible methods to track and predict right heart decompensation with pVAD support during acute heart failure in pigs and validate this approach using retrospective human data.

RESULTS

Hemodynamics across a spectrum of states, ranging from health to left and right heart collapse, were analyzed in five pigs undergoing left-sided pVAD support. All five animals survived induction of cardiogenic shock by coronary embolization with controlled and titrated injection of microspheres, and four animals achieved further pulmonary hypertension through similar use of microspheres in the pulmonary circulation. Animal #2 expired early from ventricular fibrillation cardiac arrest during pulmonary microembolization. Pulmonary vascular impedance varied with modest elevation in mean pulmonary artery pressure from postcapillary strain due to left ventricular ischemia, followed by graded and progressive increases in mean pulmonary artery pressure with each phase of pulmonary microembolization (fig. S1). Ultimately, a spectrum of biventricular loading states was generated due to varied animal responses and interim microembolization states.

Differences in systemic and pulmonary vascular mechanics

Advanced hemodynamic monitoring confirmed graded induction of left ventricular failure, followed by added right heart stress in the five animals with indwelling pVADs. The interaction between ventricular function and vascular loading state was compared for the left and right hearts. Left ventricular relaxation tracked with mean arterial pressure across the spectrum of states modeled in the animals, as did right ventricular relaxation with mean pulmonary artery pressure (Fig. 1, A and B). The correlation was stronger for the left ventricle ($R^2 = 0.77$) compared to the right ventricle ($R^2 = 0.58$). Left ventricular contraction tracked with mean arterial pressure and right ventricular contraction with mean pulmonary artery pressure (Fig. 1, C and D). Similarly, correlation was stronger for the left ventricle ($R^2 = 0.75$) compared to the right ventricle ($R^2 = 0.19$). In contrast to these measures of relaxation and contractility, which are known as load-dependent markers, the response of the left and right ventricles varied greatly for stroke work, representing the energy expended by the ventricle across the cardiac cycle. Left ventricular stroke work predictably tracked with systemic loading state (Fig. 1E). In contrast, right ventricular stroke work was highly variable and did not track with mean pulmonary artery pressure (Fig. 1F).

We also assessed the constituent elements of vascular function using the transvascular pressure gradient, resistance, compliance, and the resistance-compliance (RC) time constant to further study the
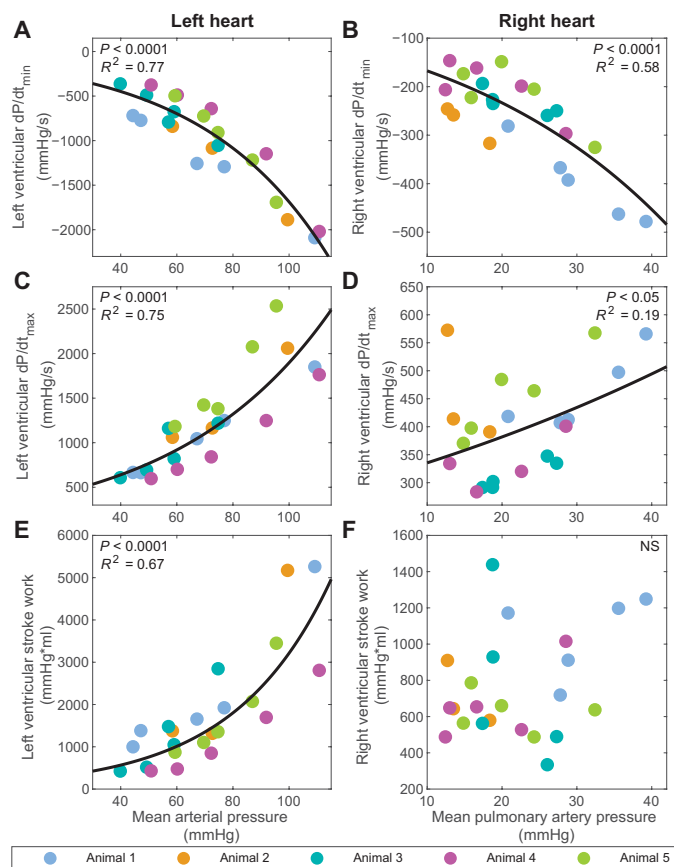

Fig. 1. Left and right ventricular function in response to systemic and pulmonary vascular load. Shown are the minimum pressure slopes, dP/dt_{min}, for the (**A**) left ($P < 0.0001$) and (**B**) right ($P < 0.0001$) ventricles across the spectrum of states modeled in the animals with pVAD support. dP/dt_{min} is a load-dependent measure of relaxation, and the panels show its alteration as mean arterial pressure and mean pulmonary artery pressure change. The maximum pressure slope, dP/dt_{max}, is shown as well for the (**C**) left ($P < 0.0001$) and (**D**) right ($P < 0.05$) ventricles across the spectrum of states. dP/dt_{max} is a load-dependent measure of contractility, and the panels show its alteration as mean arterial pressure and mean pulmonary artery pressure change. (**E**) Left ($P < 0.0001$) and (**F**) right (NS) ventricular stroke work are similarly presented related to mean arterial pressure and mean pulmonary artery pressure. $N = 23$ states modeled, with constant pVAD speed ($N = 22$ for RV dP/dt_{max} due to catheter disruption). Linear regression was performed to confirm validity of trends. Corresponding curves and the square of the multiple correlation coefficient are denoted for correlations of statistical significance, determined by P value < 0.05.

systemic and pulmonary circulations of the five animals. Distinct differences emerged between systemic and pulmonary vascular function. Cardiac output (CO) correlated positively and in a linear manner with the transsystemic pressure gradient and, in contrast, correlated with the transpulmonary pressure gradient in a negative and exponential manner (Fig. 2A). CO did not correlate with systemic vascular resistance, but there was a negative, exponential correlation with pulmonary vascular resistance (Fig. 2B). Similarly, CO did not correlate with aortic compliance but was sensitive to the pulmonary vascular state, showing a positive, linear correlation with pulmonary vascular compliance (Fig. 2C). The RC time constant represents the combined influence of vascular resistance and compliance. There was

no correlation between CO and the systemic RC time constant; however, because of the unique properties of the pulmonary vasculature, there was a negative and exponential correlation for CO with the pulmonary RC time constant (Fig. 2D).

Impact of pulmonary vascular state on pVAD utility

As the left and right ventricles are linked serially, pulmonary vascular dynamics not only affect right heart function but also the left ventricular response to pVAD support. pVAD speed sweeps were performed, with progressive ramps in device speed as tolerated, and metrics of left heart state and function were assessed. Across the speed sweeps, greater decrement in left ventricular end-diastolic volume or preload was attained in states with higher pulmonary vascular compliance, indicating that greater left ventricular unloading was achieved (Fig. 3A). Consequently, there was also greater reduction in left ventricular maximum pressure slope (dP/dt_{max}), a load-dependent measure of contractility, as well as systemic arterial elastance, a measure of afterload, in states with higher pulmonary vascular compliance (Fig. 3, B and C). Last, incorporating these cumulative effects on left ventricular state, increased pVAD support led to a greater increase in left ventricular stroke volume and a greater reduction in left ventricle stroke work at states of higher pulmonary vascular compliance (Fig. 3, D and E).

Effects of varied pVAD stimulus on right heart physiology

The transvalvular pVAD provides a means of rapidly and dynamically altering load in the heart. Previously, pVAD load modulation has been used to measure systemic vascular resistance and CO (*50*). This study extended the use of the pVAD to determine potential cardiac reserve, specifically the ability of the right heart to increase output and match the mechanically enhanced left-sided blood flow and to reveal complex heart physiology that cannot be studied without left ventricular support. At steady state, pulmonary vascular compliance had a profound impact on pulmonary arterial elastance, with decreased compliance resulting in increased right ventricular afterload (Fig. 4A). The pVAD speed sweeps revealed how this relationship between pulmonary vascular compliance and right ventricular afterload responded to rapid changes in left ventricular support at each of the states modeled (Fig. 4B). In high compliance states, there was a rapid change in pulmonary vascular compliance across the pVAD speed sweep, indicating adaptability that maintained right ventricular afterload relatively constant (Fig. 4B). In less adaptable states, however, pulmonary vascular compliance was less variable across pVAD speed sweeps, and right ventricular afterload was subject to larger changes, indicating intolerance to left-sided support (Fig. 4B).

Cardiac assessment during the pVAD speed sweep

To evaluate cardiac reserve in response to pVAD speed sweep at the bedside, metrics must be developed for assessment of pulmonary vascular function. Given that the pulmonary vasculature acted over a greater dynamic range and in a manner more complicated than ohmic resistance found in the systemic circulation, its function could be modulated as loads changed. For example, as intrathoracic pressure changed with breathing, pulmonary vascular function changed as well. Consequently, a hysteretic transpulmonary relationship emerged. Rather than a linear elastic response, changes in mean pulmonary artery pressure (upstream of the vascular bed) with respect to left ventricular end-diastolic pressure (downstream) were delayed due to capacitance loading and dissipation by pulmonary vascular compliance (Fig. 5A). This hysteresis did not occur in the transsystemic relationship, as the systemic vascular bed did not
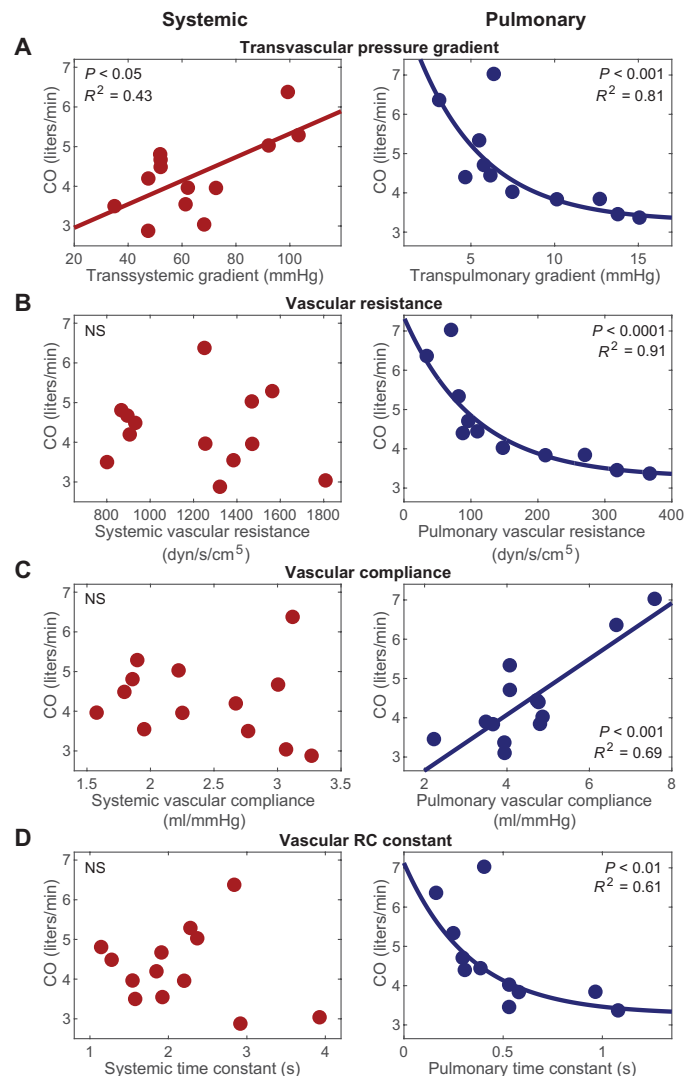

Fig. 2. Differences in systemic and pulmonary vascular mechanics. The figure presents cardiac output across the spectrum of states modeled in the five animals with pVAD support in response to four different factors: (**A**) transsystemic pressure gradient (mean arterial pressure–right ventricular end-diastolic pressure) ($P < 0.05$) and transpulmonary pressure gradient (mean pulmonary arterial pressure–left ventricular end-diastolic pressure) ($P < 0.001$), (**B**) systemic vascular resistance (NS) and pulmonary vascular resistance ($P < 0.001$), (**C**) aortic compliance (NS) and pulmonary vascular compliance ($P < 0.001$), and (**D**) systemic RC time constant (NS) and pulmonary RC time constant ($P < 0.01$). $N = 13$ states with triplicate thermodilution, with constant pVAD speed ($N = 11$ for measurements involving transpulmonary pressure gradient due to catheter disruption). Linear regression was performed to confirm validity of trends. Corresponding curves and the square of the multiple correlation coefficient are denoted for correlations of statistical significance, determined by P value < 0.05.

have the same capacity for dynamic changes in compliance (Fig. 5B). The area of these transpulmonary loops correlated with pulmonary vascular compliance, indicating that, with higher compliance, there was greater capacitance and adaptability in the system (Fig. 5C).

We implemented this measure of pulmonary vascular compliance to assess right heart adaptability and predict tolerance to pVAD support. Across the pVAD speed sweeps for the spectrum of states modeled, the percent change in transpulmonary loop area correlated with right ventricular stroke work, enabling prediction of future tolerance

Fig. 3. Pulmonary vascular compliance determines pVAD utility for left ventricular function. Shown is the degree of benefit achieved across pVAD speed sweeps for the left ventricle in relation to pulmonary vascular compliance at each of the states modeled in the animals. Left ventricular benefit was measured by changes in (**A**) left ventricular end-diastolic volume ($P < 0.001$), (**B**) left ventricular maximum pressure slope, dP/dt_{max} ($P < 0.05$), (**C**) left ventricular afterload, determined by systemic arterial elastance ($P < 0.05$), (**D**) left ventricular stroke volume ($P < 0.01$), and (**E**) left ventricular stroke work ($P < 0.01$). $N = 21$ complete pVAD speed sweeps. Corresponding curves and the square of the multiple correlation coefficient are denoted for correlations of statistical significance, determined by P value < 0.05.
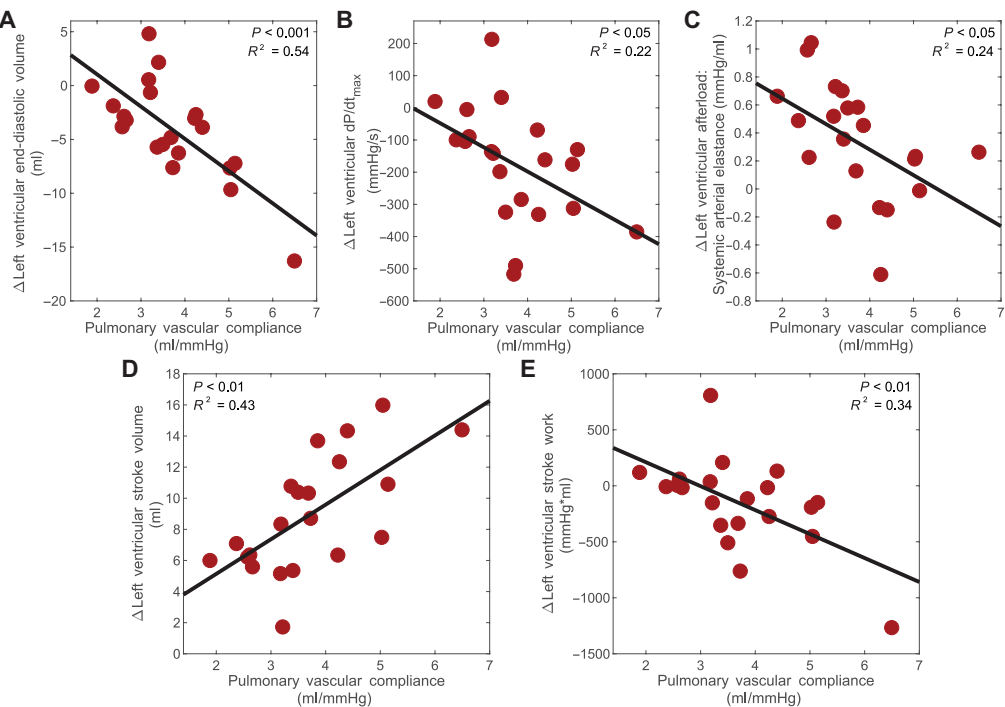

Fig. 4. pVAD stimulus indicates right heart adaptability to left ventricular support. The correlation between right ventricular afterload and pulmonary vascular compliance is shown across the range of states modeled in the five animals with pVAD support. Right ventricular afterload was measured at (**A**) static points in time and constant pVAD speed and (**B**) across pVAD speed sweeps to create a dynamic stimulus. $N = 23$ states modeled.
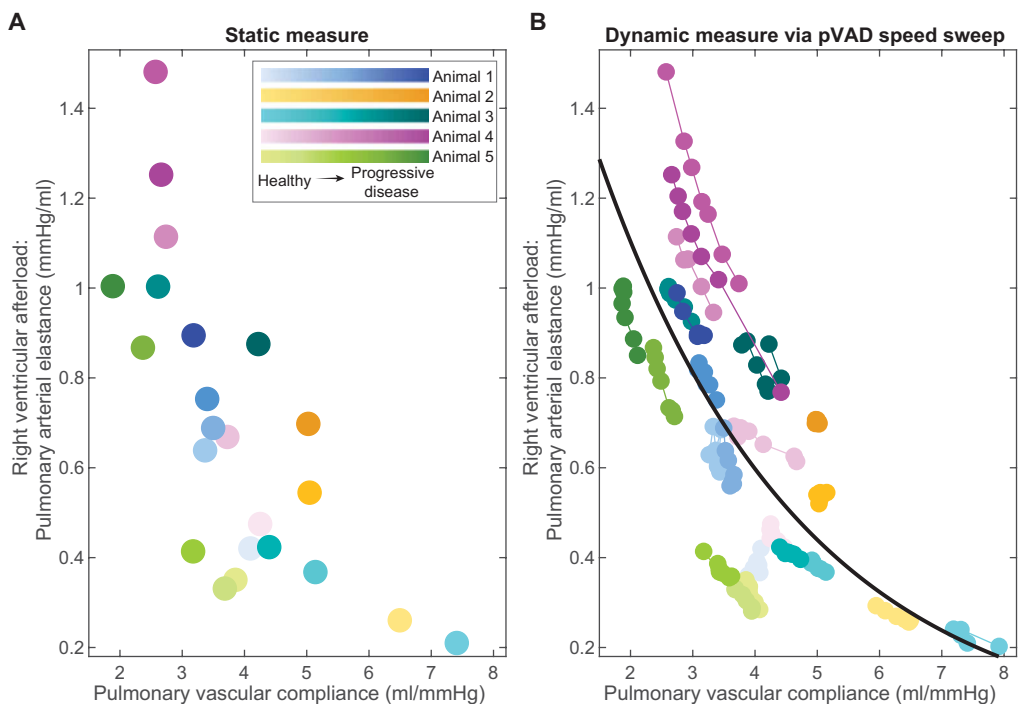
to left ventricular support before failure emerging (Fig. 5D). Furthermore, pVAD speed sweeps allowed safe and dynamic query of the system, and calculation of transpulmonary loop area for measurements of pulmonary vascular compliance could be acquired clinically with a standard right heart catheterization along with pVAD-obtained measurements of left ventricular end-diastolic pressure (*51*).

Validation of cardiac metrics with a retrospective human dataset

Porcine findings were validated by retrospective analysis of data from eight patients undergoing variable pVAD support. There were a total of 40 inquiries and 26 P-level speed changes across a range of physiologic states. Representative transpulmonary hysteresis loops
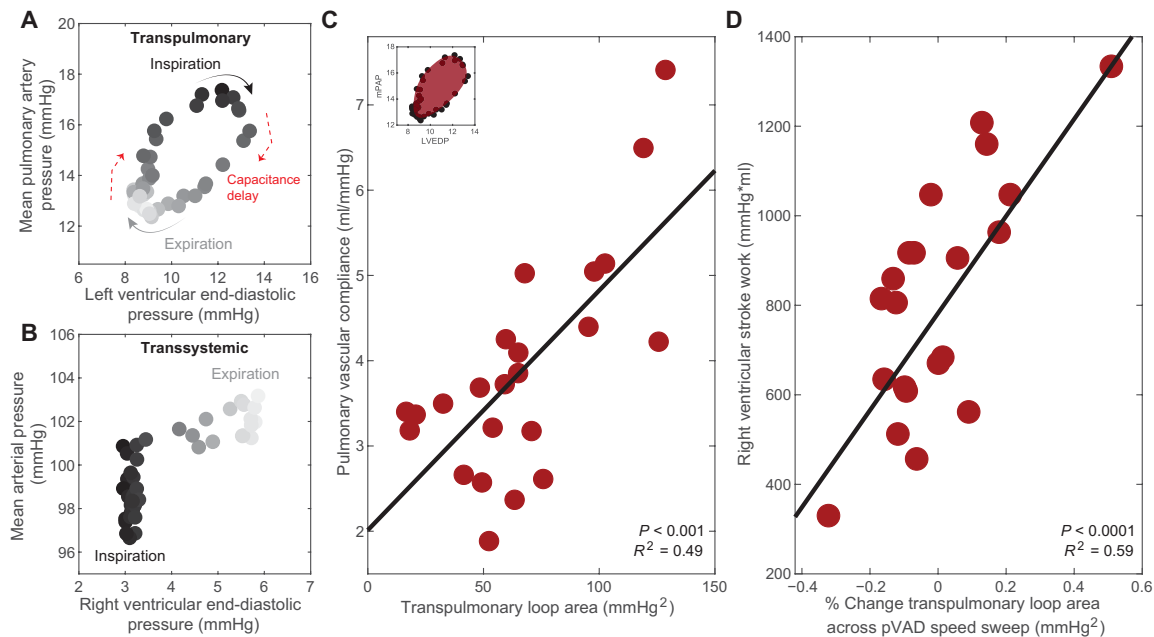
Fig. 5. Transpulmonary hysteresis measures pulmonary vascular compliance and predicts right heart tolerance. Shown is an example of (**A**) a hysteretic transpulmonary relationship between mean pulmonary artery pressure (mPAP) and left ventricular end-diastolic pressure (LVEDP) across the respiratory cycle in one animal with constant pVAD support at a steady physiological state. A corresponding example of (**B**) a nonhysteretic transsystemic relationship between mean arterial pressure and right ventricular end-diastolic pressure is similarly shown for one animal with constant pVAD support at steady state. (**C**) The relationship between pulmonary vascular compliance and area of the transpulmonary hysteresis loops is shown for the spectrum of states modeled in the five animals with pVAD support. $N = 23$ states modeled, $P < 0.001$. (**D**) The resulting correlation between right ventricular stroke work, representing right heart tolerance to pVAD support, and the percent change in transpulmonary loop area across pVAD speed sweeps is presented across the range states modeled in all animals. $N = 21$ complete pVAD speed sweeps, $P < 0.0001$. Linear regression was performed to confirm validity of trends. Corresponding curves and the square of the multiple correlation coefficient are denoted for correlations of statistical significance, determined by P value < 0.05.

at high and low pVAD speeds mimicked what was observed in the animals and confirmed that pVAD speed sweep could dynamically alter pulmonary vascular state and assess adaptability in humans (Fig. 6A). Furthermore, correlation between transpulmonary hysteresis loop area and pulmonary vascular compliance was also statistically significant ($P < 0.0001$) in the human data (Fig. 6B). Last, similar to the response in animals, the percent change in transpulmonary loop area across an increase in pVAD speed correlated with the systolic pulmonary artery pressure, which served as a surrogate for right ventricular wall stress and thus right heart tolerance to left-sided ventricular support (Fig. 6C).

DISCUSSION

VADs offer new promise for patients in cardiogenic shock by providing left ventricular support with minimal increase in energy demands for the heart. Increasing VAD use has resulted in reduced duration and severity of disease as well as native heart recovery for many patients. Despite this, mortality rates for indwelling VAD use remain high, and questions regarding optimal use—including which patients will benefit most, how to best titrate left ventricular support, and which devices are optimal—have yet to be addressed. A major limitation of VADs is the response of the right ventricle and pulmonary vasculature, with right heart failure after initiation of left-sided support remaining a critical barrier to enhanced clinical utility of these devices. Similarly, the propensity for or the presence

of pulmonary hypertension establishes further limitations and a quandary regarding fixed or dynamic vascular impedance that may affect related outcomes such as candidacy for heart transplantation. Here, we show that pVADs can be used to predict the clinical course during cardiogenic shock in a porcine model with varied right and left heart disease states. Intraventricular placement of this device creates a platform to quickly alter loads in the heart while simultaneously maintaining support of the impaired left ventricle and directly recording intraventricular functional metrics. This platform can be used as a means of dynamically stressing the right heart and revealing tolerance to stress that is unable to be assessed with traditional static metrics. By developing and using this approach in the porcine study, we enabled access to cardiac metrics that are not usually available, most notably the change in pulmonary vascular compliance, which can be measured by transpulmonary hysteresis and revealed right heart tolerance to left-sided support.

Traditionally, right and left ventricular coupling is a feature of intact cardiovascular homeostasis and enables the ventricles to support and counterbalance each other in maintaining perfusion and optimizing cardiac energetics (*5–7*). With preserved ventricular coupling, pVAD support should improve left and right heart function through clearing of passive pulmonary congestion attributed to left ventricular failure and through reduced septal impingement, thereby increasing right ventricular compliance (*22, 52–54*). However, increased left ventricular support can trigger a cycle of decompensation that affects both ventricles in the hours after initiation of
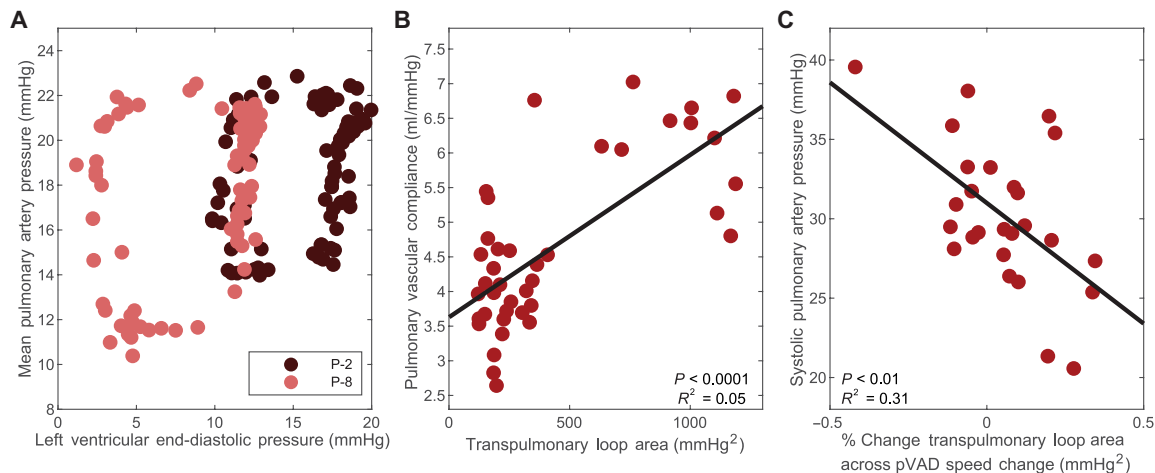
Fig. 6. Human pVAD speed sweeps validate prediction platform. Trends across pVAD speed sweeps are shown for a corresponding retrospective dataset of eight human patients with pVAD support during high-risk percutaneous coronary intervention. (**A**) Shown is an example of transpulmonary hysteresis loops for one patient at low and high pVAD speeds. (**B**) The correlation between pulmonary vascular compliance and area of the transpulmonary hysteresis loops is presented for the spectrum of states across the eight patients. $N = 40$ states assessed, $P < 0.0001$. (**C**) The corresponding trend between right heart tolerance to left ventricular support, measured by systolic pulmonary artery pressure, related to percent change in transpulmonary loop area is shown for the spectrum of states across all eight patients. $N = 26$ pVAD speed changes, $P < 0.01$. Corresponding curves and the square of the multiple correlation coefficient are denoted for correlations of statistical significance, determined by P value < 0.05.

support, if the right heart cannot accommodate these acute changes in load. This decompensation can lead to right ventricular dilation and leftward septal shift, worsening cardiac failure and reducing VAD utility (*52, 55*). Although this is a common challenge when using VADs, understanding the mechanics of this decompensation and determining metrics for its prediction remains an urgent need.

Pulmonary artery catheters often accompany mechanical circulatory support devices, although it is not entirely clear how they can be harnessed to drive device use. End-diastolic pressure as a measure of preload, pulse pressure as a surrogate for stroke volume, and mean arterial pressure and vascular resistance as measures of afterload are adequate to define the left ventricle as a pressure generator and the systemic circulation as an ohmic resistor (*56*). However, the right ventricle and pulmonary circulation differ from their left-sided counterparts, and although measurable, central venous pressure, pulmonary artery pulse pressure, pulmonary vascular resistance, and the pulmonary artery pulsatility index have limited ability to prospectively predict right heart decompensation or even the persistence of pulmonary hypertension (*57–61*). Moreover, standard metrics describe a singular state in time, limiting them in determining cardiac reserve and response to stress. Thus, tolerance to intervention requires extended periods of time and consequently is confounded by uncontrolled state changes. Consideration of mechanisms specific to the right heart and use of the pVAD as a platform for controlled stimulus to the system may aid in advanced prediction and tracking of right ventricular decompensation during mechanical circulatory support.

This study was designed to span a broad range of biventricular loading states to enable assessment of these differences in the right and left hearts and their role in ventricular coupling, specifically during pVAD support. This design also allowed for translation of the study findings to the broad range of states present in patients with cardiogenic shock. The range of biventricular loading states was generated through two forms of physiological intervention:

graded degrees of left ventricular ischemia due to controlled coronary microembolization and additional right ventricular stress due to titrated pulmonary microembolization (fig. S1). The differences in systemic and pulmonary vascular function and their contributions to right heart tolerance of left-sided pVAD unloading were analyzed.

Classically, vascular function is described using an analogy to Ohm's law, with the transvascular pressure gradient determined by the product of blood flow and vascular resistance (*62, 63*). The constituent vascular functional elements contributing to ventricular afterload suggest that the systemic vasculature is governed by the transsystemic pressure gradient, with the vascular beds resembling variable ohmic resistors in parallel and their function consisting of static compliance and neuroendocrine-mediated resistance (Figs. 1 and 2). In contrast, the pulmonary vascular metrics exhibited inverse mechanics, fitting with Permutt's description of the pulmonary circulation as a network of Starling resistors (*64–66*). Because the vessels are surrounded by the lungs, transmural pressure changes across the vessel walls can mechanically alter resistance and compliance through vessel recruitment and distension. As a result, both resistance to continuous flow and impedance to pulsatile volume load were critical to pulmonary vascular function (Fig. 2). Thus, the pulmonary circulation may act as a tuned RC circuit, and as a result, right ventricular stroke work does not track with mean pulmonary artery pressure in the same way that left ventricular stroke work tracks with mean arterial pressure (Fig. 1).

In light of the Starling resistor function of the pulmonary circulation, volume load in the pulmonary vessels is critical to right heart function. The pulmonary vascular compliance became increasingly limited in our study with progressive increases in volume load in response to pulmonary congestion from backward propagation of elevated left ventricular preload and then further with pulmonary microembolization and vessel occlusion. This handling of volume and pulsatile load creates a unique vascular adaptability in the face

Lamberti *et al.*, *Sci. Transl. Med.* **16**, eadk4266 (2024)   14 February 2024

6 of 11

of cardiopulmonary stress and, if limited, can ultimately have profound implications on the ability of the right heart to move volume in heart failure and with mechanical circulatory support.

The effect of pulmonary vascular compliance on the efficacy and degree of support achieved by the left-sided pVAD was one of these outcomes. The reduction in left ventricular preload and afterload rose with higher pulmonary vascular compliance, indicating greater improvements in left heart state achieved with the device (Fig. 3). Furthermore, the higher the pulmonary vascular compliance, the greater the benefit to left ventricular function and workload as these animals had the greatest reduction in left ventricular contraction rate and stroke work. Last, the device achieved greater increases in total left-sided stroke volume in states with higher pulmonary vascular compliance, indicating greater effectiveness in improving CO and end-organ perfusion.

Mechanical devices offer exciting potential with both their intended purpose of circulatory support and their ability to provide predictive analysis of advanced heart failure (50, 51, 67–69). It was use of the pVAD that enabled observation of these pulmonary vascular dynamics and the important role of pulmonary vascular compliance in tolerance to device support. Because of the nature of cardiovascular disease, physiological reserve is diminished, meaning that variance in the system is reduced. In addition, classic metrics describe the system solely at a static point in time. What the pVAD offers is a means of dynamically stimulating the system, creating the opportunity to assess how patient physiology will respond to stress across a broad range of loads, thereby increasing the variance in the system and expanding beyond static measurements. Moreover, monitoring of patient response to interventions traditionally requires a timescale of hours to days to determine tolerance and is confounded by uncontrolled state change. This means that the right heart response is only observed after right heart failure has emerged and the patient shows worsened symptoms of congestion, end-organ malperfusion, and device suction events. pVADs can shrink that timescale by providing different degrees of support, thereby altering loading states of the heart, while simultaneously stabilizing cardiogenic shock states. This approach creates a method to rapidly and safely test the physiologic system and determine the response on the order of minutes, eliminating the confounding uncontrolled state changes associated with longer time periods and allowing more rapid intervention to prevent full-scale right ventricular failure.

By applying a controlled pVAD stimulus in this study, we have expanded beyond classic static metrics to unveil pulmonary vascular adaptability in response to stress (Fig. 4). This response reveals right heart and pulmonary vascular tolerance to pVAD support and potentially long-term responses to interventions such as heart transplantation. In the tolerant state, pulmonary vascular function adjusted to maintain right heart afterload and allowed for matching of right ventricular output to left ventricular output. pVAD speed sweeps revealed that in cases with greater change in pulmonary vascular compliance, the right heart adapted and maintained afterload. However, with reduced adaptability, pulmonary vascular compliance was no longer responsive and coupled to changes in left ventricular preload, suggesting right ventricular intolerance to left-sided support.

One form of innate stress on the system is imposed by the respiratory cycle, with variability in vessel transmural pressure caused by intrathoracic pressure changes. Throughout this cycle, a hysteretic transpulmonary relationship was generated in both animals and humans, with a delay in pressure transmission between the pulmonary artery and the left ventricle imposed by pulmonary vascular compliance (Figs. 5 and 6), which was not observed in the systemic circulation. Leveraging this unique transpulmonary relationship, pulmonary vascular compliance was predicted by the area of these hysteretic loops, and therefore, the percent change in these areas across a pVAD speed sweep was predictive of right heart adaptability and tolerance to left ventricular unloading.

Traditional metrics related to preload, contractility, vascular resistance, and arterial elastance define state-based phenomena and are governed by classic Starling forces and Poiseuille flow but have not fully captured ventricular interactions and regulation in particular of the right heart. Advanced mechanistic understanding involving pulmonary vascular compliance can now be introduced to define the cardiovascular system within the context of stress simulated by pVAD stimuli. These therapeutic devices then can be transformed to create a hemodynamic stress test. Controlled titration of mechanical circulatory support speed can span the spectrum of future states, unmask complex right-left ventricular interactions, and reveal how a patient will respond. Furthermore, this response can be defined using the transpulmonary loop area, which is obtained with a standard right heart catheterization and pVAD-obtained continuous measurements of left ventricular end-diastolic pressure (51, 70).

By capitalizing on the unique positioning and operation of pVADs (fig. S2), the developed metrics can help predict right heart tolerance before patients exhibiting frank right ventricular decompensation. Such an approach can allow clinical teams to better titrate the degree of left-sided support provided, optimizing biventricular function (fig. S3). By rapidly assessing the response across a safe and controlled pVAD speed sweep, an inflection point in the trajectory of the developed metric could indicate the speeds that the right ventricle tolerates compared to the point at which decompensation begins. This inflection point may inform the physician of the maximum speed for titration. In the most severe cases, the response may indicate that the right ventricle is entirely intolerant to left-sided support, allowing physicians to initiate biventricular support earlier in a patient's disease course, which improves patient outcomes compared to delayed biventricular support (71, 72).

This work expands upon efforts by others to study right heart function and recognize its importance during mechanical circulatory support. Our study focuses on the importance of pulmonary vascular state for biventricular tolerance to left-sided mechanical support, and porcine models of left ventricular ischemia and pulmonary hypertension were used to vary the load in the pulmonary vasculature. Like all studies, there are limitations that must be considered. Cardiogenic shock and pulmonary vascular disease manifest in several forms and a range of extents; thus, it will be important to study right and left ventricular interactions in different animal models to validate findings across the broad spectrum of disease and shock. Human data validation of the animal experiments must be considered in light of differences between the datasets in the species we used. Although the humans, like the animals, were purposefully selected to span a wide range of ischemic and pulmonary vascular states, the animals were all ostensibly normal at baseline with no known lung or heart disease and were managed with standard and consistent ventilator settings. Last, although our study includes multiple data points in five animals and eight humans, our findings will require further validation with larger human cohorts with pVAD support to translate these findings for use at the bedside and in patient management.

MATERIALS AND METHODS

Study design

We assessed the impact of controlled pVAD stimulus on the right and left ventricles of five pigs across a spectrum of cardiovascular states. The biventricular response to pVAD speed sweep was first assessed in the intact healthy animals. It was then assessed after two gradations of left ventricular ischemia induced by coronary artery microembolization and two gradations of right ventricular strain induced by pulmonary artery microembolization. Loading states and pulmonary vascular impedances were varied to determine the role of ventricular interactions on biventricular tolerance to acute left ventricular unloading and to mechanistically inform cardiac metrics that could be used to predict this tolerance before decompensation. The animal study was approved by the CBSET Institutional Animal Care and Use Committee, Protocol Number I00294. All animals were maintained in accordance with NIH and AAALAC guidelines (CBSET) with continuous monitoring of body temperature, oxygen saturation, end-tidal carbon dioxide, and electrocardiogram. Randomization and blinding were not performed, as each subject underwent the same protocol, and all data were included.

To validate the porcine data, we retrospectively analyzed anonymized hemodynamic data from eight patients who underwent pVAD support in Asuncion, Paraguay. The protocol was reviewed and approved by the Bioethics Committee of the Office of the Superintendent of Health, Paraguay. Analysis was performed under the supervision of the Massachusetts Institute of Technology Committee on the Use of Humans as Experimental Subjects (E-4909). Each subject was enrolled after signing the Ethics Committee–approved informed consent form. The data were anonymized for analysis. Eight subjects (six male, two female; 62.6 ± 6.97 years) underwent pVAD support for an average period of 2.43 ± 1.07 hours during high-risk percutaneous coronary intervention. pVAD speed sweeps were performed before and after intervention, and continuous measurements of pulmonary artery, left ventricle, and aortic pressures and continuous CO determined by thermodilution (Edwards LifeSciences) were collected. Left ventricular end-diastolic pressure, mean pulmonary artery pressure, pulmonary vascular compliance, and systolic pulmonary artery pressure were assessed across pVAD speed sweeps, as tolerated.

Mechanical circulatory support device

The pVAD used, the Impella CP (Abiomed), is a transvalvular, catheter-mounted, mixed-flow pump. The device was introduced percutaneously through the femoral artery and advanced retrograde across the aortic valve to continuously pump blood antegrade in tandem with native output for left ventricular unloading and increased CO (fig. S2). An external controller modulated power to maintain an operator-determined fixed rotor speed. pVAD speed sweeps were performed, with progressive ramps in Impella performance level (P-Level) between P-2 and P-8 (31,000 to 44,000 revolutions per minute), as tolerated.

Animal preparation and data acquisition

A series of five acute animal trials (~75 kg Yorkshire swine; adolescent; four male, one female) was used to assess biventricular function across a range of cardiac conditions. Anesthesia was induced by intramuscular injection of tiletamine-zolazepam (4 to 6 mg/kg) and maintained using intravenous propofol (~0.2 to 0.4 mg/kg per min). Animals had no known lung disease and were maintained on a Puritan Bennett 840 Ventilator (Medtronic) in volume control mode with a tidal volume of 8 ml/kg body weight, positive end-expiratory pressure of 5 cmH$_2$O, and fraction of inspired oxygen of 50%, standard ventilatory parameters used clinically. Peak inspiratory pressures ranged from 12 to 20 cmH$_2$O, and respiratory rate was titrated to maintain an arterial partial pressure of carbon dioxide of 35 to 45 mmHg. Following each study (duration, ~8 hours), animals were euthanized in accordance with accepted American Veterinary Medical Association guidelines.

A research-grade data acquisition system (ADInstruments) continuously recorded a single-lead electrocardiogram and hemodynamic measurements from femoral, carotid, and jugular access points. Pressure-volume conductance catheters (Millar) were positioned in each ventricle. A Swan Ganz catheter was used for thermodilution CO assessment. Straight-tip pressure sensors (Millar) measured aortic and pulmonary artery pressures, along with a femoral vein external pressure transducer (ADInstruments). Fluoroscopy was used to verify device placement and monitor aortic valve competency.

Animal model

The intact biventricular response to pVAD speed sweep was first assessed. Left ventricular ischemia was then induced through injections of 0.25-ml compressible microspheres (diameter, 45 to 105 µm) (Hydropearl, Terumo) mixed with 20 ml of equal parts isotonic saline and contrast into the left anterior descending coronary artery. When initial signs of ischemia were detected through reduced coronary flow, mean arterial pressure, mixed venous oxygen saturation, and/or elevated left ventricular end-diastolic pressure, microsphere injections were paused to assess the response to pVAD sweep in this initial ischemic condition. Injections were continued to reach cardiogenic shock, defined by left ventricular end-diastolic pressure > 20 mmHg, mean arterial pressure < 60 mmHg, and/or mixed venous oxygen saturation < 55%. Additional microsphere boluses were injected into the left circumflex as needed, mindful of animal state, coronary anatomy, and degree of left anterior descending occlusion. pVAD sweeps were then conducted to assess the response under left ventricular ischemic insult alone.

Acute pulmonary hypertension was then induced through pulmonary artery microembolization to stress the right ventricle beyond postcapillary strain associated with left ventricular ischemia. Similar to the coronary microembolization approach, this model and the nature of the injectable particles allow precise control to induce graded forms of stress. Boluses of 0.01-g Sephadex microspheres (diameter, 100 to 300 µm) (Cytiva) in 2 ml of equal parts isotonic saline and contrast were repeatedly injected into the pulmonary artery to incrementally strain the right ventricle. The response to pVAD speed sweep was measured at a preliminary stage of elevated pulmonary vascular impedance and at a final pulmonary occlusion state defined by either an increase in mean pulmonary artery pressure of >10 mmHg compared to the shock state or a reduction in mean arterial pressure to <40 mmHg. Both of these indicate right ventricular stress: Elevated mean pulmonary artery pressure represents an increase in right ventricular afterload, and the reduction in mean arterial pressure occurs due to reduced flow through the pulmonary circulation into the left ventricle, thereby reducing left ventricular output.

Data analysis

Data were registered and analyzed using MATLAB (MathWorks). In the animals, five different clinical conditions were considered

including health and two gradations of coronary and pulmonary artery bead occlusions. Criteria were identified for final coronary and pulmonary occlusion states, whereas interim microembolization states were purposefully varied to generate wide-ranging biventricular functional states across a physiologic continuum, which amounted to 23 distinct physiologic states. At each state, responses were recorded at seven device speeds as tolerated between P-2 and P-8, amounting to 159 total inquiries and 21 complete pVAD speed sweeps. Hemodynamics at each state were assessed across 1 minute of steady values, and metrics were calculated for beats in sinus rhythm and stable catheter signal. Instances of catheter disturbance which precluded calculation of particular metrics are denoted in individual figure legends. In the humans, there were a total of 40 inquiries, amounting to 26 P-level speed changes for assessment.

Ventricular functional metrics include end-diastolic pressure; end-diastolic volume; maximum pressure slope (dP/dt_{max}) and minimum pressure slope (dP/dt_{min}), measures of contractility and relaxation, respectively; stroke volume; and stroke work, calculated by area of the pressure-volume loops. Vascular metrics include arterial elastance; mean arterial pressures; transvascular pressure gradient (the difference between the upstream mean arterial pressure and the downstream end-diastolic pressure); vascular resistance; vascular compliance (ratio between stroke volume and pulse pressure); and vascular RC time constant (product of vascular resistance and compliance). The time constant is a metric used with exponential behaviors, demonstrating the time to increase or decrease by 1-1/e from the initial value (73). For vascular function, this metric represents the time of exponential pressure decay during diastole (73).

Statistical analysis

Data are presented as trends along the continuum of states modeled. Linear regression was performed in Microsoft Excel, with logarithmic transform for exponential fits, to confirm validity of trends. Corresponding curves and the square of the multiple correlation coefficient are denoted for correlations of statistical significance, determined by P value < 0.05. P values are reported for all correlations as NS (not significant), $P < 0.05$, $P < 0.01$, $P < 0.001$, and $P < 0.0001$. Data in fig. S1 were analyzed with a one-way analysis of variance (ANOVA) and post hoc Tukey honest significant difference test using Prism 10.0 (GraphPad).

Supplementary Materials

This PDF file includes:
Figs. S1 to S3

Other Supplementary Material for this manuscript includes the following:
Data file S1
MDAR Reproducibility Checklist

REFERENCES AND NOTES

1. C. Vahdatpour, D. Collins, S. Goldberg, Cardiogenic Shock. *J. Am. Hear. Assoc. Cardiovasc. Cerebrovasc. Dis.* **8**, e011991 (2019).
2. H. Thiele, I. Akin, M. Sandri, G. Fuernau, S. de Waha, R. Meyer-Saraei, P. Nordbeck, T. Geisler, U. Landmesser, C. Skurk, A. Fach, H. Lapp, J. J. Piek, M. Noc, T. Goslar, S. B. Felix, L. S. Maier, J. Stepinska, K. Oldroyd, P. Serpytis, G. Montalescot, O. Barthelemy, K. Huber, S. Windecker, S. Savonitto, P. Torremante, C. Vrints, S. Schneider, S. Desch, U. Zeymer, PCI strategies in patients with acute myocardial infarction and cardiogenic shock. *N. Engl. J. Med.* **377**, 2419–2432 (2017).
3. H. Thiele, E. M. Ohman, S. de Waha-Thiele, U. Zeymer, S. Desch, Management of cardiogenic shock complicating myocardial infarction: An update 2019. *Eur. Heart J.* **40**, 2671–2683 (2019).
4. E. Lüsebrink, A. Kellnar, K. Krieg, L. Binzenhöfer, C. Scherer, S. Zimmer, B. Schrage, S. Fichtner, T. Petzold, D. Braun, S. Peterss, S. Brunner, C. Hagl, D. Westermann, J. Hausleiter, S. Massberg, H. Thiele, A. Schäfer, M. Orban, Percutaneous transvalvular microaxial flow pump support in cardiology. *Circulation* **145**, 1254–1284 (2022).
5. A. A. Bove, W. P. Santamore, Ventricular interdependence. *Prog. Cardiovasc. Dis.* **23**, 365–388 (1981).
6. W. P. Santamore, M. Constantinescu, B. M. Minczak, C. E. Hock, L. Papa, Contribution of each ventricular wall to ventricular interdependence. *Basic Res. Cardiol.* **83**, 424–430 (1988).
7. W. P. Santamore, M. Constantinescu, J. Vinten-Johansen, W. E. Johnston, W. C. Little, Alterations in left ventricular compliance due to changes in right ventricular volume, pressure and compliance. *Cardiovasc. Res.* **22**, 768–776 (1988).
8. S. R. Mehta, J. W. Eikelboom, M. K. Natarajan, R. Diaz, C. Yi, R. J. Gibbons, S. Yusuf, Impact of right ventricular involvement on mortality and morbidity in patients with inferior myocardial infarction. *J. Am. Coll. Cardiol.* **37**, 37–43 (2001).
9. B. Burstein, S. van Diepen, B. M. Wiley, N. S. Anavekar, J. C. Jentzer, Biventricular function and shock severity predict mortality in cardiac ICU patients. *Chest* **161**, 697–709 (2022).
10. S. Kuchibhotla, M. L. Esposito, C. Breton, R. Pedicini, A. Mullin, R. O'Kelly, M. Anderson, D. L. Morris, G. Batsides, D. Ramzy, M. Grise, D. T. Pham, N. K. Kapur, Acute biventricular mechanical circulatory support for cardiogenic shock. *J. Am. Heart Assoc.* **6**, e006670 (2017).
11. A. Lala, Y. Guo, J. Xu, M. Esposito, K. Morine, R. Karas, S. D. Katz, J. S. Hochman, D. Burkhoff, N. K. Kapur, Right ventricular dysfunction in acute myocardial infarction complicated by cardiogenic shock: A hemodynamic analysis of the should we emergently revascularize occluded coronaries for cardiogenic shock (SHOCK) trial and registry. *J. Card. Fail.* **24**, 148–156 (2018).
12. M. N. Kavarana, M. S. Pessin-Minsley, J. Urtecho, K. A. Catanese, M. Flannery, M. C. Oz, Y. Naka, Right ventricular dysfunction and organ failure in left ventricular assist device recipients: A continuing problem. *Ann. Thorac. Surg.* **73**, 745–750 (2002).
13. N. C. Dang, V. K. Topkara, M. Mercando, J. Kay, K. H. Kruger, M. S. Aboodi, M. C. Oz, Y. Naka, Right heart failure after left ventricular assist device implantation in patients with chronic congestive heart failure. *J. Hear. Lung Transplant.* **25**, 1–6 (2006).
14. J. C. Matthews, T. M. Koelling, F. D. Pagani, K. D. Aaronson, The right ventricular failure risk score. a pre-operative tool for assessing the risk of right ventricular failure in left ventricular assist device candidates. *J. Am. Coll. Cardiol.* **51**, 2163–2172 (2008).
15. B. A. Houston, R. J. Kalathiya, S. Hsu, R. Loungani, M. E. Davis, S. T. Coffin, N. Haglund, S. Maltais, M. E. Keebler, P. J. Leary, D. P. Judge, G. R. Stevens, J. Rickard, C. M. Sciortino, G. J. Whitman, A. S. Shah, S. D. Russell, R. J. Tedford, Right ventricular afterload sensitivity dramatically increases after left ventricular assist device implantation: A multi-center hemodynamic analysis. *J. Hear. Lung Transplant.* **35**, 868–876 (2016).
16. W. P. Santamore, L. J. Dell'Italia, Ventricular interdependence: Significant left ventricular contributions to right ventricular systolic function. *Prog. Cardiovasc. Dis.* **40**, 289–308 (1998).
17. R. J. Tedford, P. M. Hassoun, S. C. Mathai, R. E. Girgis, S. D. Russell, D. R. Thiemann, O. H. Cingolani, J. O. Mudd, B. A. Borlaug, M. M. Redfield, D. J. Lederer, D. A. Kass, Pulmonary capillary wedge pressure augments right ventricular pulsatile loading. *Circulation* **125**, 289–297 (2012).
18. M. Dupont, W. Mullens, H. N. Skouri, Z. Abrahams, Y. Wu, D. O. Taylor, R. C. Starling, W. H. W. Tang, Prognostic role of pulmonary arterial capacitance in advanced heart failure. *Circ. Heart Fail.* **5**, 778–785 (2012).
19. R. J. Tedford, Determinants of right ventricular afterload (2013 Grover Conference series). *Pulm. Circ.* **4**, 211–219 (2014).
20. N. Uriel, G. Sayer, K. Addetia, S. Fedson, G. H. Kim, D. Rodgers, E. Kruse, K. Collins, S. Adatya, N. Sarswat, U. P. Jorde, C. Juricek, T. Ota, V. Jeevanandam, D. Burkhoff, R. M. Lang, Hemodynamic ramp tests in patients with left ventricular assist devices. *JACC. Heart Fail.* **4**, 208–217 (2016).
21. K. Kotoh, K. Ishii, Y. Abe, P. Deleuze, D. Loisance, Experimental assessment of right ventricular function in normal pigs with a left ventricular assist device. *Artif. Organs* **18**, 918–922 (1994).
22. W. P. Santamore, L. A. Gray, Left ventricular contributions to right ventricular systolic function during LVAD support. *Ann. Thorac. Surg.* **61**, 350–356 (1996).
23. E. Chow, D. J. Farrar, Right heart function during prosthetic left ventricular assistance in a porcine model of congestive heart failure. *J. Thorac. Cardiovasc. Surg.* **104**, 569–578 (1992).
24. S. Shehab, S. M. Allida, P. M. Davidson, P. J. Newton, D. Robson, P. C. Jansz, C. S. Hayward, Right ventricular failure post LVAD implantation corrected with biventricular support: An in vitro model. *ASAIO J.* **63**, 41–47 (2017).
25. T. Imamura, B. Chung, A. Nguyen, D. Rodgers, G. Sayer, S. Adatya, N. Sarswat, G. Kim, J. Raikhelkar, T. Ota, T. Song, C. Juricek, V. Kagan, V. Jeevanandam, M. Mehra, D. Burkhoff, N. Uriel, Decoupling between diastolic pulmonary artery pressure and pulmonary capillary wedge pressure as a prognostic factor after continuous flow ventricular assist device implantation. *Circ. Heart Fail.* **10**, e003882 (2017).

26. J. M. Read, N. I. Azih, C. J. Peters, V. Gurtu, J. K. Vishram-Nielsen, S. P. Wright, A. C. Alba, M. J. Gregoski, N. A. Pilch, S. Hsu, M. V. Genuardi, C. Inampudi, G. R. Jackson, N. Pope, L. P. Witer, A. Kilic, B. A. Houston, S. Mak, E. Y. Birati, R. J. Tedford, Hemodynamic reserve predicts early right heart failure after LVAD implantation. *J. Heart Lung Transplant.* **41**, 1716–1726 (2022).

27. D. Saeed, R. Muslem, M. Rasheed, K. Caliskan, N. Kalampokas, F. Sipahi, A. Lichtenberg, K. Jawad, M. Borger, S. Huhn, R. Cogswell, R. John, J. Schultz, H. Shah, S. Hsu, N. A. Gilotra, P. J. Scheel, B. Tomashitis, M. El Hajj, L. Lozonschi, B. A. Houston, R. J. Tedford, Less invasive surgical implant strategy and right heart failure after LVAD implantation. *J. Heart Lung Transplant.* **40**, 289–297 (2021).

28. S. G. Drakos, L. Janicki, B. D. Horne, A. G. Kfoury, B. B. Reid, S. Clayson, K. Horton, F. Haddad, D. Y. Li, D. G. Renlund, P. W. Fisher, Risk factors predictive of right ventricular failure after left ventricular assist device implantation. *Am. J. Cardiol.* **105**, 1030–1035 (2010).

29. T. S. Kato, M. Farr, P. C. Schulze, M. Maurer, K. Shahzad, S. Iwata, S. Homma, U. Jorde, H. Takayama, Y. Naka, L. Gillam, D. Mancini, Usefulness of two-dimensional echocardiographic parameters of the left side of the heart to predict right ventricular failure after left ventricular assist device implantation. *Am. J. Cardiol.* **109**, 246–251 (2012).

30. T. Ahmad, J. M. Testani, N. R. Desai, Can big data simplify the complexity of modern medicine?: Prediction of right ventricular failure after left ventricular assist device support as a test case. *JACC. Heart Fail.* **4**, 722–725 (2016).

31. P. Atluri, A. B. Goldstone, A. S. Fairman, J. W. Macarthur, Y. Shudo, J. E. Cohen, A. L. Acker, W. Hiesinger, J. L. Howard, M. A. Acker, Y. J. Woo, Predicting right ventricular failure in the modern, continuous flow left ventricular assist device era. *Ann. Thorac. Surg.* **96**, 857–864 (2013).

32. Y. Wang, M. A. Simon, P. Bonde, B. U. Harris, J. J. Teuteberg, R. L. Kormos, J. F. Antaki, Decision tree for adjuvant right ventricular support in patients receiving a left ventricular assist device. *J. Heart Lung Transplant.* **31**, 140–149 (2012).

33. O. I. I. Soliman, S. Akin, R. Muslem, E. Boersma, O. C. Manintveld, T. Krabatsch, J. F. Gummert, T. M. M. H. De By, A. J. J. C. Bogers, F. Zijlstra, P. Mohacsi, K. Caliskan, Derivation and validation of a novel right-sided heart failure model after implantation of continuous flow left ventricular assist devices: The EUROMACS (European Registry for Patients with Mechanical Circulatory Support) right-sided heart failure risk score. *Circulation* **137**, 891–906 (2018).

34. V. Tchantchaleishvili, S. Maltais, S. Sharma, N. A. Haglund, M. E. Davis, J. Cowger, P. Shah, S. S. Desai, K. D. Aaronson, F. D. Pagani, S. M. Dunlay, J. M. Stulak, A novel, highly discriminatory risk model predicting acute severe right ventricular failure in patients undergoing continuous-flow left ventricular assist device implant. *Artif. Organs* **43**, 624–632 (2019).

35. D. Nitta, K. Kinugawa, T. Imamura, E. Amiya, M. Hatano, O. Kinoshita, K. Nawata, M. Ono, I. Komuro, A useful scoring system for predicting right ventricular assist device requirement among patients with a paracorporeal left ventricular assist device. *Int. Heart J.* **59**, 983–990 (2018).

36. J. R. Fitzpatrick, J. R. Frederick, V. M. Hsu, E. D. Kozin, M. Lou O'Hara, E. Howell, D. Dougherty, R. C. McCormick, C. A. Laporte, J. E. Cohen, K. W. Southerland, J. L. Howard, M. L. Jessup, R. J. Morris, M. A. Acker, Y. J. Woo, Risk score derived from pre-operative data analysis predicts the need for biventricular mechanical circulatory support. *J. Heart Lung Transplant.* **27**, 1286–1292 (2008).

37. C. N. Lang, K. Kaier, V. Zotzmann, P. Stachon, T. Pottgiesser, C. von zur Muehlen, M. Zehender, D. Duerschmied, B. Schmid, C. Bode, T. Wengenmayer, D. L. Staudacher, Cardiogenic shock: Incidence, survival and mechanical circulatory support usage 2007–2017-insights from a national registry. *Clin. Res. Cardiol.* **110**, 1421–1430 (2021).

38. S. S. Dhruva, J. S. Ross, B. J. Mortazavi, N. C. Hurley, H. M. Krumholz, J. P. Curtis, A. P. Berkowitz, F. A. Masoudi, J. C. Messenger, C. S. Parzynski, C. G. Ngufor, S. Girotra, A. P. Amin, N. D. Shah, N. R. Desai, Use of mechanical circulatory support devices among patients with acute myocardial infarction complicated by cardiogenic shock. *JAMA Netw. Open* **4**, e2037748 (2021).

39. M. S. Panhwar, T. Gupta, A. Karim, S. Khera, R. Puri, B. K. Nallamothu, V. Menon, U. N. Khot, D. L. Bhatt, S. R. Kapadia, S. S. Naidu, A. Kalra, Trends in the use of short-term mechanical circulatory support in the United States – An Analysis of the 2012–2015 National Inpatient Sample. *Struct. Hear.* **3**, 499–506 (2019).

40. D. Oren, R. Zilinyi, D. Lotan, M. Uriel, N. Uriel, G. Sayer, The role of temporary mechanical circulatory support as a bridge to advanced heart failure therapies or recovery. *Curr. Opin. Cardiol.* **37**, 394–402 (2022).

41. R. Stretch, C. M. Sauer, D. D. Yuh, P. Bonde, National trends in the utilization of short-term mechanical circulatory support: Incidence, outcomes, and cost analysis. *J. Am. Coll. Cardiol.* **64**, 1407–1415 (2014).

42. S. van Diepen, J. N. Katz, N. M. Albert, T. D. Henry, A. K. Jacobs, N. K. Kapur, A. Kilic, V. Menon, E. M. Ohman, N. K. Sweitzer, H. Thiele, J. B. Washam, M. G. Cohen, Contemporary management of cardiogenic shock: A scientific statement from the american heart association. *Circulation* **136**, e232–e268 (2017).

43. J. Abraham, V. Blumer, D. Burkhoff, M. Pahuja, S. Sinha, C. Rosner, E. Vorovich, G. Grafton, A. Bagnola, J. Hernandez-Montfort, N. Kapur, Heart failure-related cardiogenic shock: Pathophysiology, evaluation and management considerations: Review of heart failure-related cardiogenic shock. *J. Card. Fail.* **27**, 1126–1140 (2021).

44. G. Nersesian, F. Hennig, M. Müller, J. Mulzer, D. Tsyganenko, C. Starck, T. Gromann, V. Falk, E. Potapov, F. Schoenrath, Temporary mechanical circulatory support for refractory heart failure: The German Heart Center Berlin experience. *Ann. Cardiothorac. Surg.* **8**, 76–83 (2019).

45. F. Haertel, K. Lenk, M. Fritzenwanger, R. Pfeifer, M. Franz, N. Memisevic, S. Otto, B. Lauer, O. Weingärtner, D. Kretzschmar, G. Dannberg, J. Westphal, L. Baez, J. Bogoviku, P. C. Schulze, S. Moebius-Winkler, Rationale and design of JenaMACS—Acute hemodynamic impact of ventricular unloading using the Impella CP assist device in patients with cardiogenic shock. *J. Clin. Med.* **11**, 4623 (2022).

46. T. Balthazar, T. Adriaenssens, F. Rega, C. Vandenbriele, Pulsus alternans as a sign of right ventricular failure after left ventricular assist device implantation. *J. Card. Fail.* **26**, 1093–1095 (2020).

47. H. Alkhawam, R. Rafeedheen, E. Abo-Salem, Right ventricular failure following placement of a percutaneous left ventricular assist device. *Hear. Lung* **48**, 111–113 (2019).

48. C. Y. Chiu, R. Hättasch, D. Praeger, F. Knebel, K. Stangl, I. D. Ramirez, H. Dreger, Percutaneous biventricular Impella support in therapy-refractory cardiogenic shock. *Hear. Lung* **47**, 250–252 (2018).

49. B. J. Geller, S. S. Sinha, N. K. Kapur, M. Bakitas, L. B. Balsam, J. Chikwe, D. G. Klein, A. Kochar, S. C. Masri, D. B. Sims, G. C. Wong, J. N. Katz, S. van Diepen, American Heart Association Acute Cardiac Care and General Cardiology Committee of the Council on Clinical Cardiology, Council on Cardiopulmonary, Critical Care, Perioperative and Resuscitation; Council on Cardiovascular Radiology and Intervention, Council on Cardiovascular and Stroke Nursing; Council on Peripheral Vascular Disease; and Council on Cardiovascular Surgery and Anesthesia, Escalating and de-escalating temporary mechanical circulatory support in cardiogenic shock: A scientific statement from the American Heart Association. *Circulation* **146**, e50–e68 (2022).

50. S. P. Keller, B. Y. Chang, Q. Tan, Z. Zhang, A. El Katerji, E. R. Edelman, Dynamic modulation of device-arterial coupling to determine cardiac output and vascular resistance. *Ann. Biomed. Eng.* **48**, 2333–2342 (2020).

51. B. Y. Chang, S. P. Keller, S. S. Bhavsar, N. Josephy, E. R. Edelman, Mechanical circulatory support device-heart hysteretic interaction can predict left ventricular end diastolic pressure. *Sci. Transl. Med.* **10**, e2980 (2018).

52. D. J. Farrar, P. G. Compton, J. J. Hershon, J. D. Fonger, J. D. Hill, Right heart interaction with the mechanically assisted left heart. *World J. Surg.* **9**, 89–102 (1985).

53. J. Josiassen, O. K. L. Helgestad, N. L. J. Udesen, A. Banke, P. H. Frederiksen, J. A. Hyldebrandt, H. Schmidt, L. O. Jensen, C. Hassager, H. B. Ravn, J. E. Møller, Unloading using Impella CP during profound cardiogenic shock caused by left ventricular failure in a large animal model: Impact on the right ventricle. *Intensive Care Med. Exp.* **8**, 41 (2020).

54. J. P. Yourshaw, P. Mishra, M. C. Armstrong, B. Ramu, M. L. Craig, A. B. Van Bakel, D. H. Steinberg, T. G. DiSalvo, R. J. Tedford, B. A. Houston, Effects of percutaneous LVAD support on right ventricular load and adaptation. *J. Cardiovasc. Transl. Res.* **12**, 142–149 (2019).

55. M. Hatano, T. Jimba, T. Fujiwara, M. Tsuji, C. Bujo, J. Ishida, E. Amiya, O. Kinoshita, M. Ono, Late-onset right ventricular failure after continuous-flow left ventricular assist device implantation: Case presentation and review of the literature. *J. Cardiol.* **80**, 110–115 (2022).

56. L. S. Lilly, Ed., *Pathophysiology of Heart Disease: A Collaborative Project of Medical Students and Faculty* (Wolters Kluwer/Lippincott Williams & Wilkins, ed. 6, 2016).

57. R. Korabathina, K. S. Heffernan, V. Paruchuri, A. R. Patel, J. O. Mudd, J. M. Prutkin, N. M. Orr, A. Weintraub, C. D. Kimmelstiel, N. K. Kapur, The pulmonary artery pulsatility index identifies severe right ventricular dysfunction in acute inferior myocardial infarction. *Catheter. Cardiovasc. Interv.* **80**, 593–600 (2012).

58. C. R. Shippy, P. L. Appel, W. C. Shoemaker, Reliability of clinical monitoring to assess blood volume in critically ill patients. *Crit. Care Med.* **12**, 107–112 (1984).

59. F. Jardin, O. Gueret, O. Dubourg, J. C. Farcot, A. Margairaz, J. P. Bourdarias, Right ventricular volumes by thermodilution in the adult respiratory distress syndrome. A comparative study using two-dimensional echocardiography as a reference method. *Chest* **88**, 34–39 (1985).

60. P. L. Solda, P. Pantaleo, S. Perlini, A. Calciati, G. Finardi, M. R. Pinsky, L. Bernardi, Continuous monitoring of right ventricular volume changes using a conductance catheter in the rabbit. *J. Appl. Physiol.* **73**, 1770–1775 (1992).

61. M. R. Pinsky, S. Perlini, P. L. Solda, P. Pantaleo, A. Calciati, L. Bernardi, Dynamic right and left ventricular interactions in the rabbit: Simultaneous measurement of ventricular pressure-volume loops. *J. Crit. Care* **11**, 65–76 (1996).

62. J. M. Tobin, Toward an electrical analog of the cardiovascular system in hemorrhage. *Cardiovasc. Eng. Technol.* **12**, 526–529 (2021).

63. A. Venkateshvaran, E. Tossavainen, C. Borneteg, H. Oktay Tureli, D. Vanoli, L. H. Lund, F. Flachskampf, P. Lindqvist, A novel echocardiographic estimate of pulmonary vascular

resistance employing the hydraulic analogy to Ohm's law. *IJC Hear. Vasc.* **42**, 101121 (2022).

64. S. Permutt, J. B. Howell, D. F. Proctor, R. L. Riley, Effect of lung inflation on static pressure-volume characteristics of pulmonary vessels. *J. Appl. Physiol.* **16**, 64–70 (1961).

65. S. Permutt, B. Bromberger-Barnea, H. N. Bane, Alveolar pressure, pulmonary venous pressure, and the vascular waterfall. *Respiration* **19**, 239–260 (2004).

66. S. Permutt, R. L. Riley, Hemodynamics of collapsible vessels with tone: The vascular waterfall. *J. Appl. Physiol.* **18**, 924–932 (1963).

67. B. Y. Chang, Z. Zhang, K. Feng, N. Josephy, S. P. Keller, E. R. Edelman, Hysteretic device characteristics indicate cardiac contractile state for guiding mechanical circulatory support device use. *Intensive Care Med. Exp.* **9**, 62 (2021).

68. B. Y. Chang, S. P. Keller, E. R. Edelman, Leveraging device-arterial coupling to determine cardiac and vascular state. *I.E.E.E. Trans. Biomed. Eng.* **66**, 2800–2808 (2019).

69. B. Y. Chang, C. Moyer, A. El Katerji, S. P. Keller, E. R. Edelman, A scalable approach to determine intracardiac pressure from mechanical circulatory support device signals. *I.E.E.E. Trans. Biomed. Eng.* **68**, 905–913 (2021).

70. Study Details | The Smart Pump Study | ClinicalTrials.gov (available at https://clinicaltrials.gov/study/NCT04465201).

71. K. Takeda, Y. Naka, J. A. Yang, N. Uriel, P. C. Colombo, U. P. Jorde, H. Takayama, Outcome of unplanned right ventricular assist device support for severe right heart failure after implantable left ventricular assist device insertion. *J. Hear. Lung Transplant.* **33**, 141–148 (2014).

72. J. R. Fitzpatrick, J. R. Frederick, W. Hiesinger, V. M. Hsu, R. C. McCormick, E. D. Kozin, C. M. Laporte, E. Howell, D. Dougherty, J. E. Cohen, K. W. Southerland, J. L. Howard, E. C. Paulson, M. A. Acker, R. J. Morris, Y. J. Woo, Early planned institution of biventricular mechanical circulatory support results in improved outcomes compared with delayed conversion of a left ventricular assist device to a biventricular assist device. *J. Thorac. Cardiovasc. Surg.* **137**, 971–977 (2009).

73. S. R. Reuben, Compliance of the human pulmonary arterial system in disease. *Circ. Res.* **29**, 40–50 (1971).